UNIVERSITY OF BIRMINGHAM

HONO Measurement by Differential Photolysis

Bloss, William; Crilley, Leigh; Kramer, Louisa

[Link to publication on Research at Birmingham portal](#)

1   **HONO Measurement by Differential Photolysis**

2   **C. Reed[1], C. A. Brumby[3], L. R. Crilley[4], L. J. Kramer[4], W. J. Bloss[4], P. W. Seakins[2,3], J. D.**
3   **Lee[1,2], L. J. Carpenter[1]**

4   [1] Wolfson Atmospheric Chemistry Laboratories, Department of Chemistry, University of
5   York, Heslington, York, YO10 5DD, United Kingdom

6   [2] NCAS, School of Earth and Environment, University of Leeds, Leeds, LS2 9JT, United
7   Kingdom

8   [3] School of Chemistry, University of Leeds, Leeds, LS2 9JT, United Kingdom

9   [4] School of Geography, Earth and Environmental Sciences, University of Birmingham, B15
10   2TT, United Kingdom.

11   Correspondence to: James.Lee@york.ac.uk

12

13   **Abstract**

14   Nitrous acid (HONO) has been quantitatively measured *in-situ* by differential photolysis at 385

15   and 395 nm and subsequent detection as nitric oxide (NO) by the chemiluminescence reaction

16   with ozone (O_3). The technique has been evaluated by FT-IR to provide a direct HONO

17   measurement in a simulation chamber, and compared side-by-side with a LOng Absorption Path

18   Optical Photometer (LOPAP) in the field. The NO/O_3 chemiluminescence technique is robust,

19   well characterized and capable of sampling at low pressure whilst solid-state converter

20   technology allows for unattended *in-situ* HONO measurements in combination with fast time

21   resolution and response.

22   **1   Introduction**

23   Nitrous acid (HONO) is a major source of hydroxyl (OH) radicals in the boundary layer

24   (Elshorbany et al., 2008; Kim et al., 2014; Levy II, 1973). HONO can be formed homogeneously

25   through reaction of nitric oxide (NO) with OH, heterogeneously through several pathways, or

26   emitted directly (Kleffmann, 2007; Lammel and Cape, 1996; Spataro and Ianniello, 2014; Su et

27   al., 2011). HONO is formed heterogeneously on surfaces through the reaction of NO_2 with H_2O

28   (Bröske et al., 2003). This heterogeneous formation of HONO is a net source of OH radicals in

1   the troposphere and is an important mediator of air quality, particularly in polluted environments

2   (Finlayson-Pitts et al., 2003; Gutzwiller et al., 2002; Lee et al., 2015). Direct emission of HONO

3   through vehicle exhaust is also thought to be a source (Kirchstetter et al., 1996; Kurtenbach et

4   al., 2001). Emission from snowpack has also been documented (Beine et al., 2008; Zhou et al.,

5   2001) and more recently biogenic sources of HONO have been identified from nitrite producing

6   bacteria (Oswald et al., 2013; Su et al., 2011), and soil crusts (Weber et al., 2015).

7   In urban areas HONO can be the major net source of OH (discounting radical cycling driven by

8   e.g. NO), contributing up to 80% of daytime OH production in winter and 50% in summer

9   (Elshorbany et al., 2008; Kleffmann, 2007; Villena et al., 2011b). However, the sources of

10   HONO and the many processes by which it forms are not well understood (Kleffmann et al.,

11   2006; Sörgel et al., 2011; Spataro and Ianniello, 2014; Villena et al., 2011a). There is a clear

12   need for *in-situ* measurement of HONO in order to better understand its chemistry and

13   emissions.

14   Currently, methods of detecting HONO are either remotely through DOAS (Febo et al., 1996;

15   Hendrick et al., 2014; Stutz et al., 2010), or by filter/denuder sampling (Acker et al., 2005, 2006;

16   Febo et al., 1993, 1996; Ianniello et al., 2007). A variety of *in-situ* techniques exist, namely:

17   Quantum Cascade-Tuneable Infrared Laser Differential Absorption Spectrometer (QC-TILDAS)

18   (Lee et al., 2011); Ion Drift Chemical Ionization Mass Spectrometer (ID-CIMS) (Levy et al.,

19   2014); Ambient Ion Monitor - Ion Chromatography (AIM-IC) (Markovic et al., 2012;

20   Vandenboer et al., 2014); Stripping-Coil Visible Absorption Photometry (SC-AP) (Ren et al.,

21   2011); Negative-Ion Proton-Transfer Chemical Ionization Mass Spectrometry (NI-PT-CIMS)

22   (Roberts et al., 2010); Incoherent Broadband Cavity Enhanced Absorption Spectroscopy

23   (IBBCEAS) (Pusede et al., 2014); dedicated commercial on-line, *in-situ* measurements include

24   Dual Laser – Quantum Cascade Laser (Aerodyne Research) and, as used in this study, Long Path

25   Absorption Photometer (LOPAP) (Heland et al., 2001). LOPAP has been characterized quite

26   extensively by other authors e.g. (Clemitshaw, 2004; Kleffmann and Wiesen, 2008; Kleffmann et

27   al., 2006, 2013; Ródenas et al., 2013).

Atmospheric
Measurement
Techniques
Discussions

1   Here, we demonstrate the exploitation of a known HONO interference for photolytic NO_2

2   conversion systems (Pollack et al., 2011; Ryerson et al., 2000; Sadanaga et al., 2010, 2014;

3   Villena et al., 2012), to provide a simple photolytic technique for quantitative analysis of HONO.

4   **2   Experimental**

5   The differential photolytic HONO technique, henceforth referred to as pHONO, was developed

6   from an existing fast NO_x analyser described in section 2.1. The photolytic converter is described

7   specifically in section 2.2. Calibration is described in 2.3.

8   **2.1   Differential Photolysis instrument**

9   Measurement were performed using a dual channel Air Quality Design Inc. (Golden, Colorado,

10   USA) instrument equipped with a UV-LED based photolytic NO_2 converter – commonly referred

11   to as a Blue Light Converter (BLC) as described in Reed et al. (2015).

12   Briefly, two NO chemiluminescence analysers operate in parallel with duplicated independent

13   equipment. The analysers share a common inlet allowing for parallel calibration of each channel.

14   One channel is equipped with a photolytic NO_2 converter so that NO_x can be determined with

15   that channel whilst also measuring NO concurrently. This allows for fast (1 Hz or greater)

16   determination of NO and NO_2.

17   In order to be able to also measure HONO, the NO_x channel was redesigned so that the

18   photolytic converter (section 2.2) operates in a switching mode. That is, the two lamps of

19   different wavelengths operate alternately on a 50% duty cycle. Practically, the lamps switch

20   every 30 seconds allowing for ca. 1 minute time resolution data.

21   **2.2 NO_2/HONO photolytic converter**

22   Photolytic converters were based on those supplied by Air Quality Design and manufactured

23   according to their proprietary standards (Buhr, 2004, 2007) and are described in Reed et al.,

24   (2015). Practically, two UV-LED arrays are positioned at opposing ends of a cavity which is

25   highly reflective to UV. Sample gas is introduced at one end of the illuminated cavity, exiting at

26   the other. NO in the sample exiting the converter is enhanced over the original by photolysis of

27   NO_2 or HONO, thus by calibration of the conversion efficiency these can be quantified.

1   Modifications were made to the control of the UV-LED elements to allow independent switching

2   of the lamps. The wavelength of one lamp was changed from standard (395 nm) to 385 nm in

3   order to overlap better with the HONO absorption spectrum, while the actual UV-LEDs (3 watt,

4   LED Engin, Inc.) are more efficient and higher powered than those used in previous work (Reed

5   et al., 2015).

6   The volume of the illuminated sample chamber is 16 mL which, with a standard flow rate of 1

7   standard L per min^{-1} gives a sample residence time of 0.96 seconds at standard atmospheric

8   temperature and pressure (SATP). The $NO_2 \rightarrow NO$ conversion efficiency of the standard BLC

9   with the sample flow of 1 standard L per min^{-1} was ~89 % with both lamps illuminated.

10   Individual lamp conversion efficiencies were 72.9 and 81.3 % ±0.1 for the 385 and 395 nm

11   lamps respectively. Determination of the conversion efficiency is detailed in section 2.4.

12   **2.3   Characterisation**

13   Spectral radiograms of the UV-LEDs output were obtained using the same procedure and

14   equipment described in Reed et al., (2015) using an Ocean Optics QE65000 spectral radiometer

15   coupled to a 2π quartz collector within a light sealed chamber.

16   Figure 1 shows the measured spectral emission of two UV-LED units of two different

17   wavelengths; 385 and 395 nm. Also shown is the absorption cross-section of HONO, $BrONO_2$,

18   and the NO_2 quantum yield (Sander et al., 2006). It is clear that there is greater overlap,

19   calculated to be 30%, of the HONO absorption features with the 385 nm LED than at 395 nm. In

20   R2 we see that NO is produced stoichiometrically through the photolysis of HONO. In this way,

21   illuminating an air sample at either wavelength yields a signal, we shall denote as $NO_2^{\dagger}$; which

22   represents the sum of contributions from NO_2 and HONO (R1 + R2) in differing proportions

23   depending upon wavelength.

24   $NO_2 + h\nu(<410nm) \rightarrow NO + O(^3P)$ (R1)

25   $HONO + h\nu(<390 \text{ nm}) \rightarrow NO + OH$ (R2)

26   The difference in $NO_2^{\dagger}$ signal measured at 385 and 395 nm corresponds to the difference in

27   conversion efficiency of HONO and NO_2 between the two wavelengths. Differences in NO_2

Atmospheric
Measurement
Techniques
Discussions

1   conversion efficiency of each lamp may be readily calibrated for and so taken into account (see

2   section 2.4). The difference in $NO_2^\dagger$ signal measured at 385 and 395 nm can therefore be used to

3   calculate the HONO present in the sample Eq. (1);

4    $$\frac{NO_2{^\dagger}_{385} - NO_2{^\dagger}_{395}}{HONO\ CE_{385} - HONO\ CE_{395}} = [HONO] \tag{1}$$

5   Apparent HONO conversion efficiency (CE), HONO CE_{385} – HONO CE_{395}, is determined

6   experimentally as described in section 2.4.

7   It is noted that at both 385 nm and 395 nm there is potential interference from $BrONO_2$ (or in fact

8   any other compounds which photolyse to give NO at either wavelength), with similar spectral

9   overlap (Figure 1). Assuming a quantum yield of 1 integrated over all wavelengths for $BrONO_2$,

10   21.5 ppt of $BrONO_2$ at 385 nm and 18.1 ppt at 395 nm would be required to produce a 1 ppt

11   error in the NO_2/HONO signal. Due to the low abundance (< 10 pptV) of $BrONO_2$ in the lower

12   atmosphere (Yang et al., 2005), interference is therefore likely to be minimal (Pollack et al.,

13   2011). The difference in conversion for the different lamps equates to a maximum error in

14   HONO determination of 3.4 % [$BrONO_2$]; typically much less than 1 ppt.

15   The NO + OH back reaction after an air sample has exited the photolytic converter, but before

16   entering the high vacuum of the analyser, causing a decrease in signal from HONO is discussed

17   in Sec. 2.4.

18   **2.4   HONO and NO_2 Conversion Efficiencies**

19   The NO_2 – HONO converter system was calibrated for both NO_2 and HONO conversion

20   efficiency. NO_2 conversion efficiencies were determined following the procedure outlined by

21   Lee et al., (2009). The sensitivity of a detector in counts per second per part per trillion (cps/ppt)

22   is determined by adding a 7.5 mL min^{-1} mass flow controlled flow (MFC) of NO calibration gas

23   (4.78 ppm NO in N_2, BOC) to the inlet of the analyser whilst sampling an overflow of zero air

24   free from NO_x, VOC and ozone. This equates to a calibration concentration of 12.5 ppbV NO per

25   channel. Zero air was generated by scrubbing dried (-40 T_d) compressed air using Sofnofil

26   (Molecular Products) and activated charcoal (Sigma Aldrich) traps. As described by Reed et al.,

27   (2015) this combination results in the lowest NO_2 signal. The sensitivity was found to be ~ 6.8

1   and ~ 6.4 (±5%) cps/ppt for the NO and NO_x channels, respectively. In order to determine the

2   NO_2 converter efficiency a portion of the NO added to the inlet is first titrated to NO_2 by reaction

3   with ozone, typically generating 10.0 ppbV NO_2. Ozone is generated by illuminated a small flow

4   (~10 mL min^{-1}) of O_2 with a broad output low pressure mercury UV lamp (BHK Inc.) The

5   analyser signal (photomultiplier counts in Hz) is then recorded with neither UV-LED

6   illuminated, and then with each illuminated in turn to determine the increase in signal arising for

7   each lamp. The conversion efficiency (CE) is then determined as in Eq. (2).

8   $$CE = 1 - \frac{Signal_{Untitrated} - Signal_{Illuminated}}{Signal_{Untitrated} - Signal_{Titrated}}$$ (2)

9   The NO_2 conversion efficiency was determined to be 72.9 ($j = 1.3$ s^{-1}) and 81.2 % ($j = 1.7$ s^{-1})

10   ±0.1 for the 385 and 395 nm lamps, respectively.

11   Calibration for HONO was achieved by sampling a permeation source over a range of dilutions

12   using methods modified from Taira and Kanda, (1990) and Febo et al., (1995). Nitrous acid was

13   generated by the reaction of hydrochloric acid with sodium nitrite salt as described by Febo et

14   al., (1995) shown in reaction 3.

15   $HCl + NaNO_2 \rightarrow HONO + NaCl$ (R3)
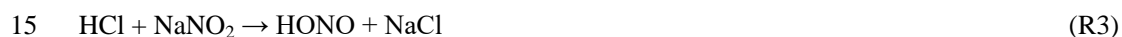
16   In order to achieve a continuous source of HONO, a permeation tube (Kin-Tek, HRT-010.00-

17   BLANK/U) was filled with HCl (37%, Fluka, AR grade) and placed in a thermostated (30 to 55

18   ^{o}C) permeation oven (Kin-Tek, 585) with $NaNO_2$ salt (Fluka, AR grade). The permeation oven

19   was flushed with 1.5 standard L min^{-1} zero air. The reaction is limited by HCl which permeates at

20   a low rate thus allowing low concentrations (<50 ppb) of HONO to be generated continuously.

21   As side products of reaction 3 can also be produced, the output of the permeation source was

22   continuously analysed for impurities. In reaction 4 NO and NO_2 can be formed by the gas phase

23   self-reaction of HONO. In reaction 5, HNO_3 can be formed by reaction between adsorbed and

24   gas phase HONO.

25   $2HONO_{(g)} \rightarrow NO + NO_2 + H_2O$ (R4)

26   $HONO_{(ads)} + NO_2 \rightarrow HNO_3 + NO$ (R5)

Atmospheric
Measurement
Techniques

Open Access

Discussions

1   To quantify HONO without any direct measurement and close the nitrogen balance, NO, NO_2,

2   and total NO_y (NO + NO_2 + other reactive oxidised nitrogen species such as HNO_3, HONO,

3   PAN) were measured continuously. The differential photolysis instrument itself was used to

4   quantify the NO. NO_2 was measured directly by Cavity Attenuated Phase Shift (CAPS)

5   spectroscopy (Kebabian et al., 2005, 2008) using an EPA certified Teledyne API T500U, to

6   avoid any HONO interference (which would have been present in a photolytic measurement).

7   Total NO_y was quantified using a Thermo Environmental 42c TL NO_x analyser equipped with a

8   molybdenum catalytic converter which has been shown to quantify NO_y species such as HONO

9   and HNO_3 (Clemitshaw, 2004; Fehsenfeld et al., 1987; Villena et al., 2012; Williams et al.,

10   1998). The TEI 42c TL and Teledyne API T500U were calibrated either directly with an NO

11   standard or by gas phase titration of NO to NO_2 using a Monitor Europe S6100 Multi Gas

12   Calibrator. Production of HNO_3 (R5) would be indicated by an enhancement in NO over NO_2, as

13   NO and NO_2 are produced stoichiometrically through the self-reaction of HONO (R4), whereas

14   HNO_3 production consumes NO_2 and produces NO. Thus, HNO_3 can be indirectly quantified by

15   the NO: NO_2 ratio, and was found to be a minimal contribution to total NO_y. As such, HONO

16   can reasonably be presumed to be equivalent to $[NO_y] - ([NO] + [NO_2] + [HNO_3])$. Measured

17   quantities are shown in table 1.

18

19   The stability of the HONO permeation source was recorded over a 12 hour period using NO_x

20   measured by the differential photolysis analyser (the most sensitive measurement available) as a

21   proxy for NO, NO_2, and HONO. The stability was found to be ±0.01 ppb h^{-1}, with a standard

22   deviation of 0.4 ppb. The uncertainty in the HONO source is determined by a combination of the

23   accuracy of the NO, NO_2, and NO_y measurements and their respective calibrations. The NO

24   calibration uncertainty, due to MFC flows and standard gas accuracy is 5%, similarly for the

25   CAPS NO_2 and Thermo 42i TL NO_y. This results in an overall uncertainty in [HONO] of 8.7%.

26   In Fig. 2 the observed conversion of HONO, that is the difference between HONO conversion by

27   the 385 and 395 nm lamps, is shown. As can be seen HONO conversion is consistently 6.54 ±

28   0.21 % more at 385nm than 395 nm.   The fact that the 'apparent HONO conversion' (HONO

29   CE_{385} – HONO CE_{395} in Eq. 1) is constant as a function of HONO means that the determination of

Atmospheric
Measurement
Techniques
Discussions

1   [HONO] should be a linear function of the difference in $NO_2^{\dagger}$ signal at 385 and 395 nm. This

2   apparent HONO conversion determines the limit of detection, which is the ability of the analyser

3   to discriminate the difference in signal arising from photolysis at the two different wavelengths

4   from photon counting noise. With an apparent conversion of 6.54 ± 0.21 % the LOD with a

5   sensitivity of 6.4 cps/ppt is 40 ppt min^{-1}. The uncertainty in the apparent conversion is a

6   combination of the uncertainty in the HONO source, and in the NO_2 conversion efficiencies of

7   the two lamps. This results in an overall uncertainty of 12.2%.

8   The effect of the back reaction of OH + NO, reforming HONO, before detection of NO, thus

9   reducing the NO signal in the NO_x/HONO measurement in the presence of HONO was

10 calculated using a box model in FACSMILE kinetic modelling software (MCPA Software Ltd.).

11 Kinetic data for O_x, HO_x, and NO_x reactions taken from IUPAC Evaluated Kinetic Data

12 (Atkinson et al., 2004). The residence time between an air sample exiting the photolysis cell and

13 entering the high vacuum of the NO analyser through the ~ 25 cm of ¼ inch PFA tubing is 0.11

14 s. The air sample is a mixture of mostly NO, O_3, OH, and unconverted NO_2. The absence of UV

15 irradiation results in chemistry analogous to night-time NO_x chemistry with the addition of a

16 significant OH source. The box model was initiated with NO, NO_3, O_3, and OH concentrations

17 calculated to be at the outlet of the photolysis cell at each of the eight calibration points shown

18 previously. The interference from the OH + NO reaction was determined as the decrease in

19 [NO] during the 0.11 s residence time as a percentage of measured [HONO]. The discrepancy

20 was calculated to vary linearly with [HONO] from -0.97 to -2.10 %, with differences between

21 lamps well within the accuracy of the calibration. The degree of interference from OH in NO_2

22 and HONO determination was found to be a function of $k([OH]+[NO])$ on the timescale here

23 (0.11 s). Reducing the residence time after the photolysis cell would reduce the error in HONO

24 and NO_2 (in the presence of HONO). Conversely, a system with a suitably long residence time

25 between the photolysis cell and detector may experience little-to-no HONO interference as the

26 OH + NO back reaction begins to dominate. There is of course a trade off in that the data must

27 be corrected for ambient ozone affecting the NO:NO_2 ratio. It is important to note that there can

28 never be any negative interference in NO_2 caused by the presence of HONO, only positive or

29 none.

1   Outside of calibration the effect of the OH back reaction with NO is likely to be less significant

2   due to the presence of volatile organic compounds (VOCs) which also react with OH with

3   comparable rates to NO. It is therefore difficult to know the absolute HONO conversion of each

4   UV-LED without very accurate OH reactivity/VOC concentration measurements. Due to these

5   unknowns, it would not be possible to correct the NO_2 signal for HONO interference as might be
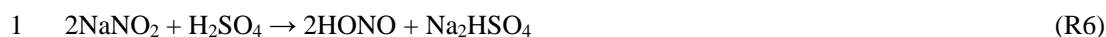
6   hoped.

7   **3   Results and discussion**

8   The pHONO instrument was evaluated in an atmospheric simulation chamber (section 3.1) and

9   compared in the field side-by-side with LOPAP (section 3.2).

10   **3.1   Chamber measurements**

11   The Highly Instrumented Reactor for Atmospheric Chemistry (HIRAC) is a simulation chamber

12   facility based at the School of Chemistry, University of Leeds (Glowacki et al., 2007a). HIRAC

13   is a cylindrical stainless steel chamber with a total volume of ~2.25 m^3, containing four fans for

14   mixing throughout the chamber, and with a total mixing time of ~60 s. The stainless steel

15   structure of HIRAC allows for pressure dependent experiments to be carried out, over the range

16   of ~10 – 1000 mbar. Numerous sample ports are located around the chamber allowing the

17   attaching of instruments or introduction of gas. A multi pass Fourier Transform - Infrared (FT-

18   IR) instrument (Bruker IFS/66, 128.52 m path length) is present to allow spectra of the gas

19   within the chamber to be taken (Glowacki et al., 2007b). HIRAC is also capable of operating

20   over a range of temperatures (-40 to 70°C).

21   Experiments were carried out at ambient temperature (20 ^{o}C) and pressure (1000 mbar), whilst

22   the chamber was kept dark. HIRAC was filled with 80 % N_2 (BOC, UHP, 99.998 %) and 20 %

23   O_2 (BOC) before HONO was synthesised external to the chamber following a modified

24   procedure described previously by (Taira and Kanda, 1990). A 1 % aqueous sodium nitrite

25   solution was added dropwise to a 30 % aqueous solution of sulfuric acid. The resulting reaction

26   (R6) produces HONO, which was added directly to the chamber via a continuous flow of N_2

27   over the reaction mixture. This is analogous to the permeation source however, side products

28   need not be considered due to the direct HONO measurement afforded by FT-IR.

Atmospheric
Measurement
Techniques
Open Access
Discussions
EGU

1    $2NaNO_2 + H_2SO_4 \rightarrow 2HONO + Na_2HSO_4$ (R6)

2   FT-IR spectra were taken at 60 second intervals with a spectral resolution of 1 cm^{-1}, whilst the

3   differential photolysis analyser sampled from the chamber. Dilution of the HONO, NO, NO$_2$

4   mixture was achieved by partial evacuation of the chamber and subsequent refilling with

5   synthetic air (N$_2$/O$_2$). The average HONO concentration determined from the average of two

6   distinct absorbance lines at 1264 cm^{-1} (*trans*-HONO, Q-branch) and 853 cm^{-1} (*cis*-HONO, Q-

7   Branch) in the FT-IR using absorptivity data taken from University of Wuppertal internal FT-IR

8   cross-section database, courtesy of I. Bejan via personal communication. The absorptivity data

9   were $7.60 \times 10^{-4} \pm 2.90 \times 10^{-5}$ ppm^{-1} m^{-1} (1264 cm^{-1}, *tans*-HONO) and $5.48 \times 10^{-4} \pm 2.60 \times 10^{-5}$ ppm^{-1}

10   m^{-1} (853 cm^{-1}, *cis*-HONO). Some of the spectra used in quantification are shown in Fig. 3.

11   Figure 4 shows the strong, positive correlation between the HONO measured by differential

12   photolysis and by FT-IR within the HIRAC chamber up to ~ 150 ppbV, deviating at higher

13   mixing ratios.

14   Figure 4 shows that at lower HONO mixing ratios, < 150 ppb, there is better agreement between

15   the pHONO and FT-IR measurements, whereas the response of the differential photolysis

16   technique appears to be suppressed at high [HONO]. This is a result of how a photolytic

17   converter operates as expressed by Eq. (3) (Ryerson et al., 2000). Here t is the residence time

18   within the photolysis cell and k[Ox] is the concentration and rate constant of any oxidant that

19   reacts with NO. Typically this would be ozone, however, OH formed from HONO photolysis

20   must also be considered.

21    $CE = \left[\dfrac{jt}{jt+k[\mathrm{Ox}]t}\right]\left[1 - exp^{(-jt-k[\mathrm{Ox}]t)}\right]$ (3)

22   Having two LEDs with different HONO absorption overlap results in two values for j(HONO).

23   Using the j(NO$_2$) values already found (1.3 & 1.7 s^{-1}) as an easily determined proxy for j(HONO)

24   the change in conversion with oxidant concentration can be approximated.

25   Figure 5 shows how the percentage conversion of any precursor that dissociates to NO, in this

26   case HONO and NO$_2$, changes with increasing oxidant concentration. In the case of O$_3$ the total

27   conversion decreases linearly with increasing [Ox], whilst the difference between the two

Atmospheric
Measurement
Techniques
Discussions

1   remains constant (9%). Conversely, with OH, conversion decays exponentially in total, and as a

2   difference between two LEDs of different j. This effect can be seen clearly above 150 ppbV

3   HONO in Fig. 4. Below 150 ppbV a constant difference in conversion of 6.54% is a reasonable

4   approximation.

5   The high HONO mixing ratios within HIRAC, necessary to be detected by FT-IR (LOD ~ 40

6   ppb), were several orders of magnitude higher than would be expected in the atmosphere where

7   ppt (Beine et al., 2006; Ren et al., 2010; Zhang et al., 2009, 2012) to low ppb (Acker et al., 2006;

8   Febo et al., 1996; Hendrick et al., 2014; Kanaya et al., 2007; Stutz, 2004) are typical. Thus, this

9   non-linearity at high [HONO] is unlikely to pose a serious limitation of the differential

10   photolysis method, with the possible exception of areas with very high NO_x backgrounds. This

11   could be partially mitigated by having greater photolysis power at 385 nm, in combination with

12   moving to shorter wavelengths with better overlap with the HONO absorption cross-section. It is

13   clear in Fig. 1 that the 385 nm UV-LED has significantly lower light output than at 395 nm; this

14   is reflected in their respective NO_2 conversion efficiencies (72.9 and 81.3%). Alternatively,

15   separate 385 and 395 nm converters can be employed working in parallel, thus doubling the

16   number of UV-LEDs and doubling the photolysis power at each respective wavelength. This

17   would also allow for fast measurement simultaneously i.e. 1 Hz or faster. Alternatively, the

18   lower conversion efficiency at high [HONO] could be calibrated for, though as shown in the

19   following section, in typical atmospheric conditions no calibration or correction was required.

20   **3.2   Field measurements**

21   The Weybourne Atmospheric Observatory (Penkett et al., 1999) is a regional GAW station

22   located on the North Norfolk coast, UK (52°57'01.5"N 1°07'19"E). The WAO has a long history

23   of atmospheric measurements stretching back to its inception in 1994. During summer 2015, the

24   WAO was host to the Integrated Chemistry of Ozone in the Atmosphere (ICOZA) campaign,

25   ostensibly measuring ozone production rates. As part of the campaign a Long Path Absorption

26   Photometer (LOPAP-03, QUMA GmbH) (Heland et al., 2001) was deployed in order to measure

27   HONO. Alongside the LOPAP, the NO, NO_2, HONO (Differential photolysis) instrument

28   described in section 2.1 measured concurrently at a 1 minute time resolution.

1   During the ICOZA campaign, a high variation of HONO concentrations (up to ~ 500 ppt) was

2   observed by the LOPAP on the 1st and 2nd of July providing an ideal opportunity for comparison

3   between the two methods. The pHONO was deployed with replacement UV-LEDs with greater

4   output. Both the 385 and 395 nm lamps had the same photon flux, indicated by identical NO_2

5   conversion efficiencies (~ 89%), in the expectation that better HONO conversion, and therefore

6   sensitivity, would be achieved. The estimated increase in overlap with the HONO adsorption

7   spectrum of the new 385 nm LED was 45% compared to 30% calculated for the original LED.

8   Thus lamps were installed as-is without calibration to mitigate the fall in output over time that

9   affects the LEDs, particularly the 385 nm LED. The decreasing output is believed to be a result

10   of the power control circuitry of the LEDs which does not limit the current draw immediately

11   after power is supplied, only after a few seconds. This means every time the lamp is switched on

12   it outputs its maximum (with corresponding heat), which, when used in a 30 s^{-1} switching mode

13   as here shortens the life considerably.

14   The pHONO instrument sampled from an inlet box (also housing a NO_y converter) located ~ 4 m

15   from ground level on the sampling tower at Weybourne. The sample point was connected to the

16   instrument by a 12 m ¼ inch PFA line (Swagelok) which was shared by the CAPS NO_2

17   instrument, thus the flowrate was ~ 3 standard L min^{-1}, resulting in a residence time of ~ 3

18   seconds. The LOPAP instrument, which has its own inlet, sampled from the roof of a specially

19   converted van located 20 m away upslope. Consequently, both instruments sampled at a similar

20   height and there was clear, unobstructed line-of-sight between them. The pHONO inlet was only

21   ~1 m above the Weybourne observatory roof which may have contributed to the turbulent

22   dynamics observed in the data. The pHONO instrument was calibrated for sensitivity in ambient

23   air twice nightly at 00:00 and 04:00 am; NO offset was taken between these times. NO_2

24   conversion efficiencies were determined in zero air once per week. Limits of detection were 1.5

25   ppt min^{-1} and 1.9 ppt min^{-1} for NO and NO_2, respectively. The LOPAP was operated and

26   calibrated according to the standard procedures described in Kleffmann and Wiesen, (2008), with

27   a detection limit of 3 pptV and time resolution of 5 minutes. Zero measurements using high

28   purity N_2 (N5 grade, BOC) were performed every 12 hours on the LOPAP.

29   Figure 6 shows the HONO time series from both the LOPAP and pHONO instruments during

30   three days of high HONO measurements.

1   There is reasonable agreement between the established LOPAP method of HONO measurement

2   and that provided by the pHONO instrument without correction or calibration (Fig. 6). During

3   the high ozone and high HONO events observed on the 1st and 2nd especially there is very good

4   agreement between the two. Gaps in the data represent times where the pHONO limit of

5   determination was reached; where there are too few points in the averaging window after

6   statistical analysis of the data to be meaningful. This is because in real atmospheric conditions

7   the pHONO instrument is hampered by the time resolution that data is collected i.e. if there is

8   strong turbulence, meaning the NO_2 or HONO concentration varies rapidly on a timescale

9   shorter than that at which data is collected, then wide scatter is observed as was the case at

10 Weybourne. Strong boundary layer transport meant that NO_2 measurement varied up to 1.5 ppb

11 in a minute. This is because of the way the data must be processed by interpolating between

12 measurements and subtraction of the 395 nm signal form the 385 nm signal. Decreasing the time

13 between photolysis switching (from 30 s) would obviously decrease this effect, but ultimately,

14 separate 385 nm (or lower) and 395 nm analyser channels are required. Consequently the data

15 analysis routine for the pHONO data includes tests for the variability of the data, discarding

16 points which show >5% variation from the subsequent point. Data failing this test is discarded

17 and results in gaps; this is the effective limit of determination. The data is then treated with a

18 robust-LOESS (Cleveland, 1979) algorithm to remove extreme values. The gaps in the time

19 series of LOPAP (Fig 5) were due to the removal of zero measurements and false spikes due to

20 bubbles passing the detector.

21 Figure 7 demonstrates the level of agreement in the measured HONO concentration by the

22 LOPAP and pHONO methods from 1st and 2nd July. From Fig. 7, the observed correlation (r^2 of

23 0.68) suggests the replacement UV-LEDs had the desired effect without the application of

24 corrections for the HONO conversion efficiency. The slope of ~ 0.91 suggests that the new 385

25 nm lamp was able to convert the majority of HONO. The discrepancy suggests that ~ 9% of

26 HONO was converted by the 395 nm lamp. The scatter evident in Fig. 7 at low mixing ratios

27 may be due to atmospheric dynamic effects resulting in a rapidly changing NO_2 background on

28 timescales faster than the response of the instrument (30 s^{-1}). A positive 5 pptV positive

29 intercept indicates a small systematic off-set in the pHONO instrument.

Atmospheric
Measurement
Techniques
Discussions

1 Accuracy and uncertainty in unstable conditions could be improved by measuring at the two

2 different wavelengths concurrently, rather than consecutively. In the same way photolytic NO_2

3 measurement is improved by measuring concurrently with NO, rather than consecutively. This

4 would require three chemiluminescent analysers in parallel, with two photolytic converters.

5 However, in ambient indoor air quality monitoring, where HONO is seen as increasingly

6 important (Gligorovski, 2016), a simple single channel, dual wavelength design might be

7 appropriate and useful.

8 **4   Conclusions**

9 An instrument for *in*-situ determination of HONO photolytically has been developed,

10 characterized and deployed in the field as a proof-of-concept. During an atmospheric simulation

11 chamber comparison, the HONO measured corresponded well with FT-IR measurement. During

12 field tests the photolytic HONO instrument agreed reasonably well with the established LOPAP

13 instrument, though the limitations of having a 2-channel sequential measurement were apparent

14 at times; this would be easily overcome in a 3-channel concurrent system. Calibration would

15 gain from a pure HONO source; currently the pHONO calibration requires an independent, direct

16 NO_2 measurement and NO_y measurement.

25 **References**

26 Acker, K., Febo, A., Trick, S., Perrino, C., Bruno, P., Wiesen, P., Möller, Wieprecht, W., Auel,
27 R., Giusto, M., Geyer, A., Platt, U. and Allegrini, I.: Nitrous acid in the urban area of Rome,
28 Atmos. Environ., 40(17), 3123–3133, doi:10.1016/j.atmosenv.2006.01.028, 2006.

Atmospheric
Measurement
Techniques
Open Access

EGU

Discussions

1 Acker, K., Möller, D., Auel, R., Wieprecht, W. and Kalaß, D.: Concentrations of nitrous acid,
2 nitric acid, nitrite and nitrate in the gas and aerosol phase at a site in the emission zone during
3 ESCOMPTE 2001 experiment, Atmos. Res., 74(1-4), 507–524,
4 doi:10.1016/j.atmosres.2004.04.009, 2005.

5 Atkinson, R., Baulch, D. L., Cox, R. A., Crowley, J. N., Hampson, R. F., Hynes, R. G., Jenkin,
6 M. E., Rossi, M. J. and Troe, J.: Evaluated kinetic and photochemical data for atmospheric
7 chemistry: Volume I - gas phase reactions of O_x, HO_x, NO_x and SO_x species, Atmos. Chem.
8 Phys., 4(6), 1461–1738, doi:10.5194/acp-4-1461-2004, 2004.

9 Beine, H., Colussi, A. J., Amoroso, A., Esposito, G., Montagnoli, M. and Hoffmann, M. R.:
10 HONO emissions from snow surfaces, Environ. Res. Lett., 3(4), 045005, doi:10.1088/1748-
11 9326/3/4/045005, 2008.

12 Beine, H. J., Amoroso, A., Domine, F., King, M. D., Nardino, M., Ianniello, A. and France, J. L.:
13 Surprisingly small HONO emissions from snow surfaces at Browning Pass, Antarctica, Atmos.
14 Chem. Phys., 6, 2569–2580, doi:10.5194/acp-6-2569-2006, 2006.

15 Bröske, R., Kleffmann, J. and Wiesen, P.: Heterogeneous conversion of NO2 on secondary
16 organic aerosol surfaces: A possible source of nitrous acid (HONO) in the atmosphere?, Atmos.
17 Chem. Phys., 3(3), 469–474, doi:10.5194/acp-3-469-2003, 2003.

18 Buhr, M.: Measurement of NO2 in ambient air using a solid-state photolytic converter, in
19 Symposium on Air Quality Measurement Methods and Technology 2004. 20 - 22 April 2004, pp.
20 165–171, Cary, NC, USA., 2004.

21 Buhr, M.: Solid-state light source photolytic nitrogen dioxide converter, US 7238328 B2, 3 July
22 2007.

23 Clemitshaw, K. C.: A Review of Instrumentation and Measurement Techniques for Ground-
24 Based and Airborne Field Studies of Gas-Phase Tropospheric Chemistry, Crit. Rev. Environ. Sci.
25 Technol., 34(1), 1–108, doi:10.1080/10643380490265117, 2004.

26 Cleveland, W. S.: Robust Locally Weighted Regression and Smoothing Scatterplots, J. Am. Stat.
27 Assoc., 74(368), 829–836, doi:10.2307/2286407, 1979.

28 Elshorbany, Y. F., Kurtenbach, R., Wiesen, P., Lissi, E., Rubio, M., Villena, G., Gramsch, E.,
29 Rickard, A. R., Pilling, M. J. and Kleffmann, J.: Oxidation capacity of the city air of Santiago,
30 Chile, Atmos. Chem. Phys. Discuss., 8(6), 19123–19171, doi:10.5194/acpd-8-19123-2008, 2008.

31 Febo, A., Perrino, C. and Allegrini, I.: Measurement of Nitrous Acid in Milan , Italy, By Doas
32 and Diffusion Denuders, Atmos. Environ., 30(21), 3599–3609, doi:10.1016/1352-
33 2310(96)00069-6, 1996.

34 Febo, A., Perrino, C. and Cortiello, M.: A denuder technique for the measurement of nitrous acid
35 in urban atmospheres, Atmos. Environ. Part A. Gen. Top., 27(11), 1721–1728,
36 doi:10.1016/0960-1686(93)90235-Q, 1993.

37 Febo, A., Perrino, C., Gherardi, M. and Sparapani, R.: Evaluation of a High-Purity and High-
38 Stability Continuous Generation System for Nitrous Acid, Environ. Sci., 29(9), 2390–2395,
39 doi:10.1021/es00009a035, 1995.

40 Fehsenfeld, F. C., Dickerson, R. R., Hobler, G., Luke, W. T., Nunnermacker, L. J., Roberts, J.

Atmospheric
Measurement
Techniques
Discussions

M., Curran, C. M., Eubank, C. S., Fahey, D. W., Mindplay, P. C. and Pickering, K. E.: A Ground-Based Intercomparison of NO, NOx, and NOy Measurement Techniques, J. Geophys. Res., 92(7), 710–722, doi:10.1029/JD092iD12p14710, 1987.

Finlayson-Pitts, B. J., Wingen, L. M., Sumner, A. L., Syomin, D. and Ramazan, K. A.: The heterogeneous hydrolysis of NO2 in laboratory systems and in outdoor and indoor atmospheres: An integrated mechanism, Phys. Chem. Chem. Phys., 5(2), 223–242, doi:10.1039/B208564J, 2003.

Gligorovski, S.: Nitrous acid (HONO): An emerging indoor pollutant, J. Photochem. Photobiol. A Chem., 314, 1–5, doi:10.1016/j.jphotochem.2015.06.008, 2016.

Glowacki, D. R., Goddard, A., Hemavibool, K., Malkin, T. L., Commane, R., Anderson, F., Bloss, W. J., Heard, D. E., Ingham, T., Pilling, M. J. and Seakins, P. W.: Design of and initial results from a highly instrumented reactor for atmospheric chemistry (HIRAC), Atmos. Chem. Phys. Discuss., 7, 10687–10742, doi:10.5194/acpd-7-10687-2007, 2007a.

Glowacki, D. R., Goddard, A. and Seakins, P. W.: Design and performance of a throughput-matched, zero-geometric-loss, modified three objective multipass matrix system for FTIR spectrometry, Appl. Opt., 46(32), 7872–7883, doi:10.1364/AO.46.007872, 2007b.

Gutzwiller, L., Arens, F., Baltensperger, U., Gäggeler, H. W. and Ammann, M.: Significance of semivolatile diesel exhaust organics for secondary HONO formation, Environ. Sci. Technol., 36(4), 677–682, doi:10.1021/es015673b, 2002.

Heland, J., Kleffmann, J., Kurtenbach, R. and Wiesen, P.: A new instrument to measure gaseous nitrous acid (HONO) in the atmosphere, Environ. Sci. Technol., 35(15), 3207–3212, doi:10.1021/es000303t, 2001.

Hendrick, F., Clémer, K., Wang, P., De Mazière, M., Fayt, C., Gielen, C., Hermans, C., Ma, J. Z., Pinardi, G., Stavrakou, T., Vlemmix, T. and Van Roozendael, M.: Four years of ground-based MAX-DOAS observations of HONO and NO2 in the Beijing area, Atmos. Chem. Phys., 14(2), 765–781, doi:10.5194/acp-14-765-2014, 2014.

Ianniello, A., Beine, H. J., Landis, M. S., Stevens, R. K., Esposito, G., Amoroso, A. and Allegrini, I.: Comparing field performances of denuder techniques in the high Arctic, Atmos. Environ., 41(8), 1604–1615, doi:10.1016/j.atmosenv.2006.10.040, 2007.

Kanaya, Y., Cao, R., Akimoto, H., Fukuda, M., Komazaki, Y., Yokouchi, Y., Koike, M., Tanimoto, H., Takegawa, N. and Kondo, Y.: Urban photochemistry in central Tokyo: 1. Observed and modeled OH and HO$_2$ radical concentrations during the winter and summer of 2004, J. Geophys. Res., 112(D21), D21312, doi:10.1029/2007JD008670, 2007.

Kebabian, P. L., Herndon, S. C. and Freedman, A.: Detection of nitrogen dioxide by cavity attenuated phase shift spectroscopy, Anal. Chem., 77(2), 724–728, doi:10.1021/ac048715y, 2005.

Kebabian, P. L., Wood, E. C., Herndon, S. C. and Freedman, A.: A practical alternative to chemiluminescence-based detection of nitrogen dioxide: Cavity attenuated phase shift spectroscopy, Environ. Sci. Technol., 42(16), 6040–6045, doi:10.1021/es703204j, 2008.

Kim, S., VandenBoer, T. C., Young, C. J., Riedel, T. P., Thornton, J. A., Swarthout, B., Sive, B.,

Atmospheric
Measurement
Techniques
Discussions

1 Lerner, B. M., Gilman, J. B., Warneke, C., Roberts, J. M., Guenther, A., Wagner, N. L., Dubé,
2 W. P., Williams, E. J. and Brown, S. S.: The primary and recyling sources of OH during the
3 NACHTT-2011 campaign: HONO as an important OH primary source in the wintertime, J.
4 Geophys. Res. Atmos., 119(11), 6886–6896, doi:10.1002/2013JD021272.Received, 2014.

5 Kirchstetter, T. W., Harley, R. A. and Littlejohn, D.: Measurement of Nitrous Acid in Motor
6 Vehicle Exhaust, Environ. Sci. Technol., 30(9), 2843–2849, doi:10.1021/es960135y, 1996.

7 Kleffmann, J.: Daytime sources of nitrous acid (HONO) in the atmospheric boundary layer,
8 ChemPhysChem, 8(8), 1137–1144, doi:10.1002/cphc.200700016, 2007.

9 Kleffmann, J., Lörzer, J. C., Wiesen, P., Kern, C., Trick, S., Volkamer, R., Rodenas, M. and
10 Wirtz, K.: Intercomparison of the DOAS and LOPAP techniques for the detection of nitrous acid
11 (HONO), Atmos. Environ., 40(20), 3640–3652, doi:10.1016/j.atmosenv.2006.03.027, 2006.

12 Kleffmann, J., Villena Tapia, G., Bejan, I., Kurtenbach, R. and Wiesen, P.: NO2 Measurement
13 Techniques: Pitfalls and New Developments, edited by I. Barnes and K. J. Rudziński, NATO
14 Sci. Peace Secur. Ser. C Environ. Secur., 120(2), 15–28, doi:10.1007/978-94-007-5034-0, 2013.

15 Kleffmann, J. and Wiesen, P.: Technical note: Quantification of interferences of wet chemical
16 HONO LOPAP measurements under simulated polar conditions, Atmos. Chem. Phys., 8(22),
17 6813–6822, doi:10.5194/acp-8-6813-2008, 2008.

18 Kurtenbach, R., Becker, K. H., Gomes, J. A. G., Kleffmann, J., Lörzer, J. C., Spittler, M.,
19 Wiesen, P., Ackermann, R., Geyer, A. and Platt, U.: Investigations of emissions and
20 heterogeneous formation of HONO in a road traffic tunnel, Atmos. Environ., 35(20), 3385–3394,
21 doi:10.1016/S1352-2310(01)00138-8, 2001.

22 Lammel, G. and Cape, J. N.: Nitrous acid and nitrite in the atmosphere, Chem. Soc. Rev., 25(5),
23 361, doi:10.1039/cs9962500361, 1996.

24 Lee, B. H., Wood, E. C., Zahniser, M. S., McManus, J. B., Nelson, D. D., Herndon, S. C.,
25 Santoni, G. W., Wofsy, S. C. and Munger, J. W.: Simultaneous measurements of atmospheric
26 HONO and NO2 via absorption spectroscopy using tunable mid-infrared continuous-wave
27 quantum cascade lasers, Appl. Phys. B Lasers Opt., 102(2), 417–423, doi:10.1007/s00340-010-
28 4266-5, 2011.

29 Lee, J. D., Moller, S. J., Read, K. A., Lewis, A. C., Mendes, L. and Carpenter, L. J.: Year-round
30 measurements of nitrogen oxides and ozone in the tropical North Atlantic marine boundary layer,
31 J. Geophys. Res., 114, doi:10.1029/2009JD011878, 2009.

32 Lee, J. D., Whalley, L. K., Heard, D. E., Stone, D., Dunmore, R. E., Hamilton, J. F., Young, D.
33 E., Allan, J. D., Laufs, S. and Kleffmann, J.: Detailed budget analysis of HONO in central
34 London reveals a missing daytime source., 2015.

35 Levy II, H.: Photochemistry of minor constituents in the troposphere, Planet. Space Sci., 21(4),
36 575–591, doi:10.1016/0032-0633(73)90071-8, 1973.

37 Levy, M., Zhang, R., Zheng, J., Zhang, A. L., Xu, W., Gomez-Hernandez, M., Wang, Y. and
38 Olaguer, E.: Measurements of nitrous acid (HONO) using ion drift-chemical ionization mass
39 spectrometry during the 2009 SHARP field campaign, Atmos. Environ., 94(2), 231–240,
40 doi:10.1016/j.atmosenv.2014.05.024, 2014.

1   Markovic, M. Z., VandenBoer, T. C. and Murphy, J. G.: Characterization and optimization of an
2   online system for the simultaneous measurement of atmospheric water-soluble constituents in the
3   gas and particle phases, J. Environ. Monit., 14(7), 1872, doi:10.1039/c2em00004k, 2012.

4   Oswald, R., Behrendt, T., Ermel, M., Wu, D., Su, H., Cheng, Y., Breuninger, C., Moravek, A.,
5   Mougin, E., Delon, C., Loubet, B., Pommerening-Röser, A., Sörgel, M., Pöschl, U., Hoffmann,
6   T., Andreae, M. O., Meixner, F. X. and Trebs, I.: HONO emissions from soil bacteria as a major
7   source of atmospheric reactive nitrogen., Science, 341(6151), 1233–5,
8   doi:10.1126/science.1242266, 2013.

9   Penkett, S. a., Plane, J. M. C., Comes, F. J., Clemitshaw, K. C. and Coe, H.: The Weybourne
10   Atmospheric Observatory, J. Atmos. Chem., 33(2), 107–110, doi:10.1023/A:1026428102821,
11   1999.

12   Pollack, I. B., Lerner, B. M. and Ryerson, T. B.: Evaluation of ultraviolet light-emitting diodes
13   for detection of atmospheric NO2 by photolysis - chemiluminescence, J. Atmos. Chem., 65(2-3),
14   111–125, doi:10.1007/s10874-011-9184-3, 2011.

15   Pusede, S. E., Gentner, D. R., Wooldridge, P. J., Browne, E. C., Rollins, A. W., Min, K.-E.,
16   Russell, A. R., Thomas, J., Zhang, L., Brune, W. H., Henry, S. B., DiGangi, J. P., Keutsch, F. N.,
17   Harrold, S. A., Thornton, J. A., Beaver, M. R., St. Clair, J. M., Wennberg, P. O., Sanders, J.,
18   Ren, X., VandenBoer, T. C., Markovic, M. Z., Guha, A., Weber, R., Goldstein, A. H. and Cohen,
19   R. C.: On the temperature dependence of organic reactivity, nitrogen oxides, ozone production,
20   and the impact of emission controls in San Joaquin Valley, California, Atmos. Chem. Phys.,
21   14(7), 3373–3395, doi:10.5194/acp-14-3373-2014, 2014.

22   Reed, C., Evans, M. J., Di Carlo, P., Lee, J. D. and Carpenter, L. J.: Interferences in photolytic
23   NO2 measurements: explanation for an apparent missing oxidant?, Atmos. Chem. Phys.
24   Discuss., 15(20), 28699–28747, doi:10.5194/acpd-15-28699-2015, 2015.

25   Ren, X., Gao, H., Zhou, X., Crounse, J. D., Wennberg, P. O., Browne, E. C., LaFranchi, B. W.,
26   Cohen, R. C., McKay, M., Goldstein, A. H. and Mao, J.: Measurement of atmospheric nitrous
27   acid at Blodgett Forest during BEARPEX2007, Atmos. Chem. Phys., 10(13), 6501,
28   doi:10.5194/acp-10-6283-2010, 2010.

29   Ren, X., Sanders, J. E., Rajendran, a., Weber, R. J., Goldstein, a. H., Pusede, S. E., Browne, E.
30   C., Min, K. E. and Cohen, R. C.: A relaxed eddy accumulation system for measuring vertical
31   fluxes of nitrous acid, Atmos. Meas. Tech., 4(10), 2093–2103, doi:10.5194/amt-4-2093-2011,
32   2011.

33   Roberts, J. M., Veres, P., Warneke, C., Neuman, J. A., Washenfelder, R. A., Brown, S. S.,
34   Baasandorj, M., Burkholder, J. B., Burling, I. R., Johnson, T. J., Yokelson, R. J. and De Gouw,
35   J.: Measurement of HONO, HNCO, and other inorganic acids by negative-ion proton-transfer
36   chemical-ionization mass spectrometry (NI-PT-CIMS): Application to biomass burning
37   emissions, Atmos. Meas. Tech., 3, 981–990, doi:10.5194/amt-3-981-2010, 2010.

38   Ródenas, M., Muñoz, A., Alacreu, F., Brauers, T., Dorn, H.-P., Kleffmann, J. and Bloss, W.:
39   Assessment of HONO Measurements: The FIONA Campaign at EUPHORE, in Disposal of
40   Dangerous Chemicals in Urban Areas and Megacities, NATO Science for Peace & Security
41   Series C: Environmental Security, pp. 45–58., 2013.

Atmospheric
Measurement
Techniques

Open Access

EGU

Discussions

1 Ryerson, T. B., Williams, E. J. and Fehsenfeld, F. C.: An efficient photolysis system for fast-
2 response NO2 measurements, J. Geophys. Res., 105(2), 26,447–26,461,
3 doi:10.1029/2000JD900389, 2000.

4 Sadanaga, Y., Fukumori, Y., Kobashi, T., Nagata, M., Takenaka, N. and Bandow, H.:
5 Development of a selective light-emitting diode photolytic NO2 converter for continuously
6 measuring NO2 in the atmosphere, Anal. Chem., 82(2), 9234–9239, doi:10.1021/ac101703z,
7 2010.

8 Sadanaga, Y., Suzuki, K., Yoshimoto, T. and Bandow, H.: Direct measurement system of
9 nitrogen dioxide in the atmosphere using a blue light-emitting diode induced fluorescence
10 technique., Rev. Sci. Instrum., 85(6), 064101, doi:10.1063/1.4879821, 2014.

11 Sander, S. P., Golden, D. M., Kurylo, M. J., Moorgat, G. K., Keller-Rudek, H., Wine, P. H.,
12 Ravishankara, A. R., Kolb, C. E., Molina, M. J., Finlayson-Pitts, B. J., Huie, R. E., and Orkin, V.
13 L.: Chemical Kinetics and Photochemical Data for Use in Atmospheric Studies, Evaluation No.
14 17, JPL Publication 10-6, Jet Propulsion Laboratory, Pasadena, USA, available at:
15 http://jpldataeval.jpl.nasa.gov (last access: 3 December 2015), 2011Sörgel, M., Regelin, E.,
16 Bozem, H., Diesch, J.-M., Drewnick, F., Fischer, H., Harder, H., Held, A., Hosaynali-Beygi, Z.,
17 Martinez, M. and Zetzsch, C.: Quantification of the unknown HONO daytime source and its
18 relation to NO2, Atmos. Chem. Phys., 11(20), 10433–10447, doi:10.5194/acp-11-10433-2011,
19 2011.

20 Spataro, F. and Ianniello, A.: Sources of atmospheric nitrous acid: State of the science, current
21 research needs, and future prospects, J. Air Waste Manage. Assoc., 64(11), 1232–1250,
22 doi:10.1080/10962247.2014.952846, 2014.

23 Stutz, J.: Relative humidity dependence of HONO chemistry in urban areas, J. Geophys. Res.,
24 109(D3), D03307, doi:10.1029/2003JD004135, 2004.

25 Stutz, J., Oh, H. J., Whitlow, S. I., Anderson, C., Dibb, J. E., Flynn, J. H., Rappenglück, B. and
26 Lefer, B.: Simultaneous DOAS and mist-chamber IC measurements of HONO in Houston, TX,
27 Atmos. Environ., 44(33), 4090–4098, doi:10.1016/j.atmosenv.2009.02.003, 2010.

28 Su, H., Cheng, Y., Oswald, R., Behrendt, T., Trebs, I., Meixner, F. X., Andreae, M. O., Cheng,
29 P., Zhang, Y. and Pöschl, U.: Soil nitrite as a source of atmospheric HONO and OH radicals.,
30 Science, 333(6049), 1616–8, doi:10.1126/science.1207687, 2011.

31 Taira, M. and Kanda, Y.: Continuous generation system for low-concentration gaseous nitrous
32 acid, Anal. Chem., 633(15), 630–633, doi:10.1021/ac00205a018, 1990.

33 Vandenboer, T. C., Markovic, M. Z., Sanders, J. E., Ren, X., Pusede, S. E., Browne, E. C.,
34 Cohen, R. C., Zhang, L., Thomas, J., Brune, W. H. and Murphy, J. G.: Evidence for a nitrous
35 acid (HONO) reservoir at the ground surface in Bakersfield, CA, during CalNex 2010, J.
36 Geophys. Res. Atmos., 119, 9093–9106, doi:10.1002/2013JD020971.Received, 2014.

37 Villena, G., Bejan, I., Kurtenbach, R., Wiesen, P. and Kleffmann, J.: Development of a new
38 Long Path Absorption Photometer (LOPAP) instrument for the sensitive detection of NO2 in the
39 atmosphere, Atmos. Meas. Tech., 4, 1663–1676, doi:10.5194/amt-4-1663-2011, 2011a.

40 Villena, G., Bejan, I., Kurtenbach, R., Wiesen, P. and Kleffmann, J.: Interferences of commercial
41 NO$_2$ instruments in the urban atmosphere and in a smog chamber, Atmos. Meas. Tech., 5(1),

Atmospheric
Measurement
Techniques

Open Access

Discussions

EGU

1   149–159, doi:10.5194/amt-5-149-2012, 2012.

2   Villena, G., Kleffmann, J., Kurtenbach, R., Wiesen, P., Lissi, E., Rubio, M. A., Croxatto, G. and
3   Rappenglück, B.: Vertical gradients of HONO, NOx and O3 in Santiago de Chile, Atmos.
4   Environ., 45(23), 3867–3873, doi:10.1016/j.atmosenv.2011.01.073, 2011b.

5   Weber, B., Wu, D., Tamm, A., Ruckteschler, N., Rodríguez-Caballero, E., Steinkamp, J.,
6   Meusel, H., Elbert, W., Behrendt, T., Sörgel, M., Cheng, Y., Crutzen, P. J., Su, H. and Pöschl,
7   U.: Biological soil crusts accelerate the nitrogen cycle through large NO and HONO emissions in
8   drylands, Proc. Natl. Acad. Sci., 112(50), 201515818, doi:10.1073/pnas.1515818112, 2015.

9   Williams, E. J., Baumann, K., Roberts, J. M., Bertman, S. B., Norton, R. B., Fehsenfeld, F. C.,
10   Sprinston, S. R., Nunnermacker, L. J., Newman, L., Olszyna, K., Meagher, J. F., Hartsell, B.,
11   Edgerton, E. S., Pearson, J. R. and Rodgers, M. O.: Intercomparison of ground-based NOy
12   measurement techniques, J. Geophys. Res., 103(17), 22261–22280, doi:10.1029/98JD00074,
13   1998.

14   Yang, X., Cox, R. A., Warwick, N. J., Pyle, J. A., Carver, G. D., O'Connor, F. M. and Savage,
15   N. H.: Tropospheric bromine chemistry and its impacts on ozone: A model study, J. Geophys.
16   Res., 110(D23), D23311, doi:10.1029/2005JD006244, 2005.

17   Zhang, N., Zhou, X., Bertman, S., Tang, D., Alaghmand, M., Shepson, P. B. and Carroll, M. a.:
18   Measurements of ambient HONO concentrations and vertical HONO flux above a northern
19   Michigan forest canopy, Atmos. Chem. Phys., 12(17), 8285–8296, doi:10.5194/acp-12-8285-
20   2012, 2012.

21   Zhang, N., Zhou, X., Shepson, P. B., Gao, H., Alaghmand, M. and Stirm, B.: Aircraft
22   measurement of HONO vertical profiles over a forested region, Geophys. Res. Lett., 36(15), 1–5,
23   doi:10.1029/2009GL038999, 2009.

24   Zhou, X., Beine, H. J., Honrath, R. E., Fuentes, J. D., Simpson, W., Shepson, P. B. and
25   Bottenheim, J. W.: Snowpack Photochemical Production of HONO: a Major Source of OH in the
26   Arctic Boundary Layer, Geophys. Res. Lett., 28(21), 4087–4090, doi:10.1029/2001GL013531,
27   2001.

28

29

Atmospheric
Measurement
Techniques
Open Access
EGU
Discussions
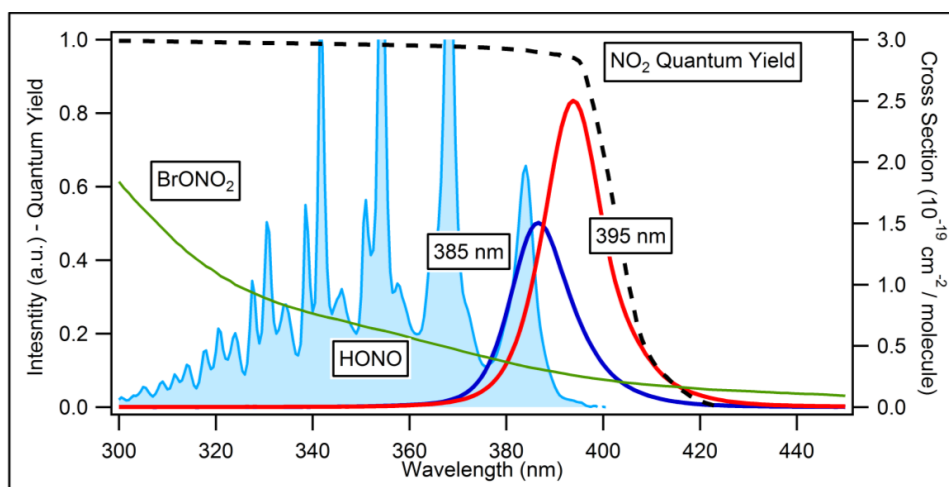
1

2   Figure 1. The measured spectral output of two UV-LED elements, nominally 385 nm output in

3   dark blue, and 395 nm in red. The HONO absorption spectrum is shown in light blue whilst the

4   NO$_2$ quantum yield is shown in dashed black. The absorption cross section of BrONO$_2$ is shown

5   in green.

6

7

1   Table 1. Showing the distribution of NO_y species NO, NO_2, HNO_3, and HONO produced from

2   the HONO permeation source.

#	NO_y ppb Measured	NO ppb Measured	NO_2 ppb Measured	HNO_3 ppb Calculated	HONO ppb Calculated
1	20.40	3.34	2.64	0.35	14.08
2	19.29	2.96	2.35	0.30	13.68
3	16.82	2.59	2.10	0.26	11.89
4	14.95	2.27	1.87	0.20	10.62
5	13.40	2.05	1.73	0.16	9.45
6	12.15	1.86	1.58	0.14	8.57
7	11.09	1.70	1.46	0.12	7.81
8	10.17	1.60	1.35	0.11	7.14
Percent	%	15.5	12.8	1.3	70.4

3
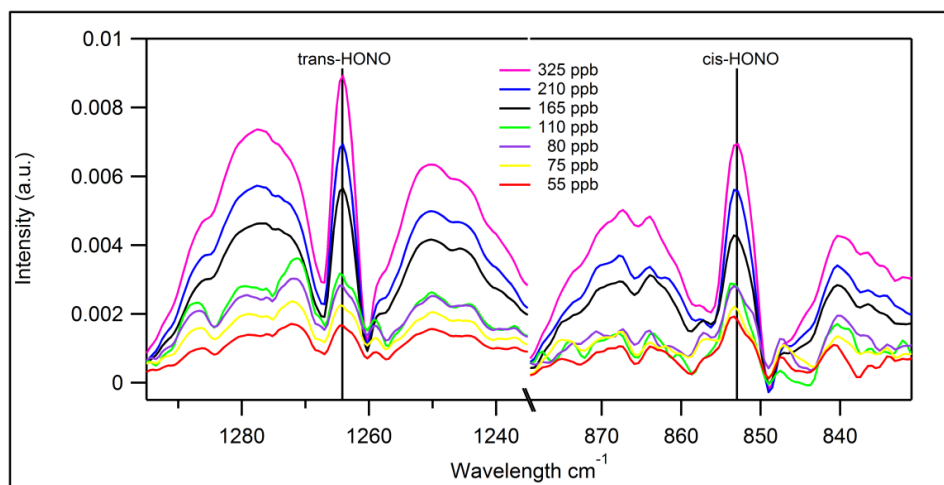
4

Atmospheric
Measurement
Techniques
Discussions
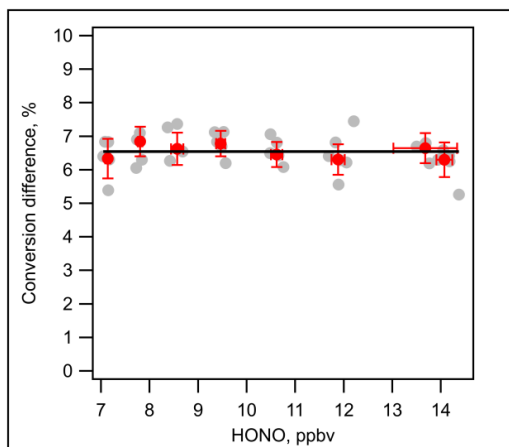
1

2   Figure 2. Difference in HONO conversion between 385 and 395 nm UV-LEDs over a range of

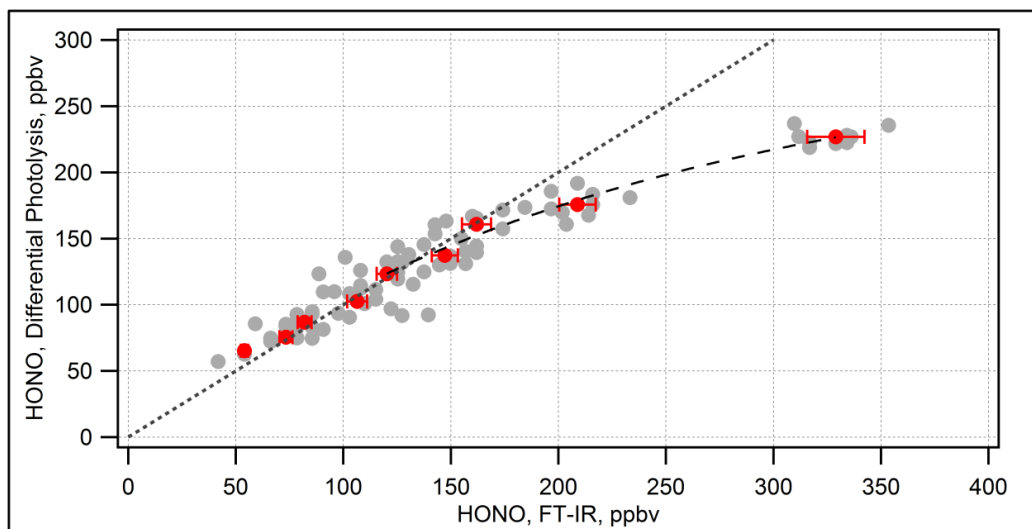3   dilutions. Median values are in red, while all data is shown in grey. Linear fit is in black.

4

Atmospheric
Measurement
Techniques

Open Access

Discussions

EGU

1

2   Figure 3. FT-IR spectra of dominant HONO absorbance lines at 1264, 853cm^{-1}, over a range of
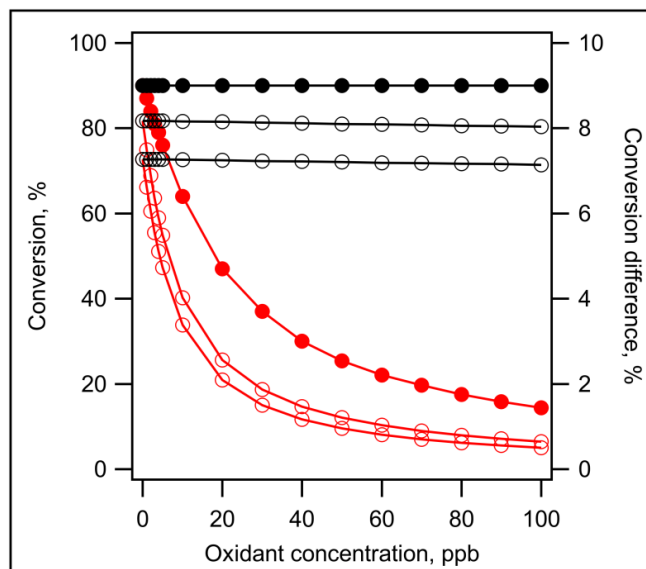
3   concentrations.

4

1

2   Figure 4. HONO determined by FT-IR (y-axis), versus HONO measured by the

3   photolytic/chemiluminescence differential photolysis instrument (x-axis). Median values at each

4   dilution are in red; all values are shown in grey. The 1:1 line is shown for reference as well as an
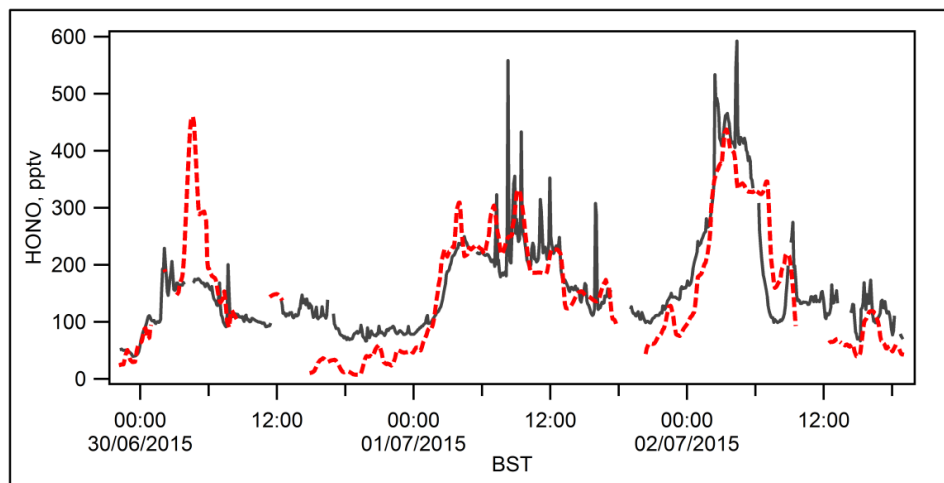
5   exponential fit above 150 ppbV HONO.

6

1

2   Figure 5. Simulated conversion (open circles), and different in conversion (closed circles) for

3   photolytic converters with different j in the presence of OH (red) and O_3 (black) oxidants.
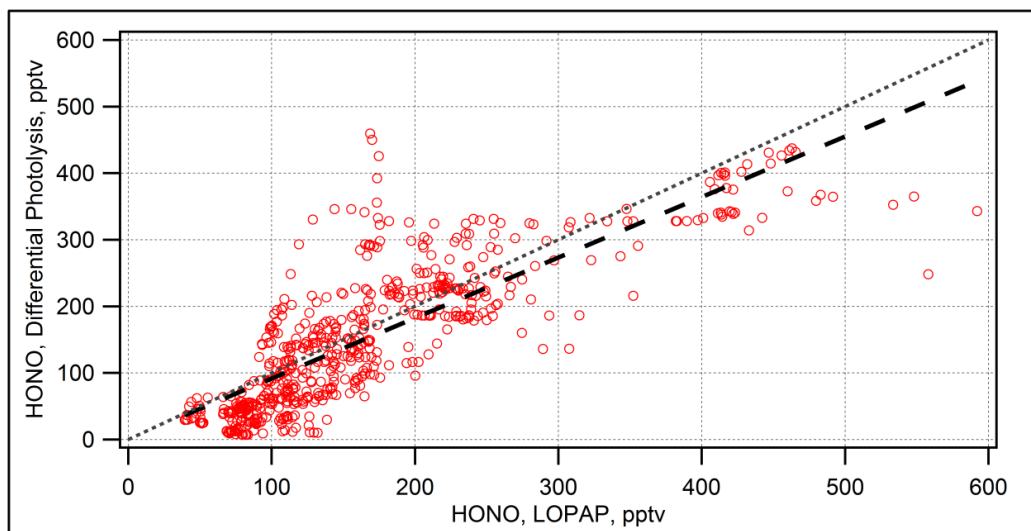
4

1

2   Figure 6. HONO time series during July 2015 at the Weybourne Atmospheric Observatory

3   (WAO) measured by LOPAP (grey) and pHONO (red).

4

1

2   Figure 7. Correlation between HONO measured by LOPAP (x-axis) and pHONO (y-axis). The

3   linear correlation is shown in black and the 1:1 line is shown for reference.

4